Anal. Chem. **2006,** *78,* 2802−2809

IMS−IMS and IMS−IMS−IMS/MS for Separating Peptide and Protein Fragment Ions

Samuel I. Merenbloom,† Stormy L. Koeniger,† Stephen J. Valentine,‡ Manolo D. Plasencia,† and David E. Clemmer*,†

Department of Chemistry, Indiana University, Bloomington, Indiana 47405, and Predictive Physiology and Medicine, Bloomington, Indiana 47405

Multidimensional ion mobility spectrometry (IMS−IMS and IMS−IMS−IMS) techniques have been combined with mass spectrometry (MS) and investigated as a means of generating and separating peptide and protein fragment ions. When fragments are generated inside a drift tube and then dispersed by IMS prior to MS analysis, it is possible to observe many features that are not apparent from MS analysis alone. The approach is demonstrated by examining fragmentation patterns arising from electrospray ion distributions of insulin chain B and ubiquitin. The multidimensional IMS approach makes it possible to select individual components for collisional activation and to disperse fragments based on differences in mobility prior to MS analysis. Such an approach makes it possible to observe many features not apparent by MS analysis alone.

Mass spectrometry techniques (MS and MS/MS) for identifying proteins based on fragmentation data (top-down and bottom-up) are transforming the study of biological systems.[1−3] It is routine to identify a protein from the pattern of tryptic peptides that is produced upon enzymatic digestion.[4−7] Once isolated, a precursor ion may be activated in order to produce a series of fragments that can be used to determine sequence. Although the progress in this area is impressive, MS/MS-based assignments often rely on fragments that are associated with only a limited region of the polypeptide sequence—the most favorable dissociation channels.[8−10] Less abundant ions are often obscured by more abundant species. This congestion of peaks is especially problematic in the dissociation of multiply charged ions, where fragmentation patterns are convoluted over multiple charge states.

Recently, we have developed a multidimensional ion mobility spectrometry (IMS) technique that makes it possible to separate and select ions based on their gas-phase mobilities prior to activation and additional stages of IMS and MS analysis.[11] In this paper, we examine the fragmentation of insulin chain B (ICB) and ubiquitin ions produced by electrospray ionization (ESI). We find that upon mobility separation it is possible to observe many peaks that were not apparent from analysis by MS alone. These additional features expand the region of sequence that is characterized and thus appear to be a useful approach for improving the protein identification with MS techniques.

The present work is closely related to a report in which we used IMS−MS methods to examine fragments of ICB and ubiquitin that were produced by MS/MS in an ion trap.[12] We note that, although many of the resulting spectra appear similar to the previously published data, the present instrument (which uses no mass spectrometer prior to the IMS instrument) has much higher resolution and sensitivity. Additionally, we find that it is possible to efficiently select specific ions for fragmentation (from the distribution of ions produced by ESI or from fragmentation of selected precursors) based on differences in their gas-phase mobilities [rather than mass-to-charge (m/z) values]. Other approaches for reducing the interference of species that coexist over limited m/z ranges include high-resolution techniques, such as Fourier transform MS,[13,14] and ion/ion reaction strategies[15] that

* To whom correspondence should be addressed. E-mail: clemmer@indiana.edu.

† Indiana University.

‡ Predictive Physiology and Medicine.

(1) For reviews, see: Biemann, K. *Annu. Rev. Biochem.* **1992**, *61*, 977−1010. McLafferty, F. W.; Kelleher, N. L.; Begley, T. P.; Fridriksson, E. K.; Zubarev, R. A.; Horn, D. M. *Curr. Opin. Chem. Biol.* **1998**, *2*, 571−578. Reid, G. E.; McLuckey, S. A. *J. Mass Spectrom.* **2002**, *37*, 663−675. Zhu, H.; Bilgin, M.; Snyder, M. *Annu. Rev. Biochem.* **2003**, *72*, 783−812. Aebersold, R.; Mann, M. *Nature* **2003**, *422*, 198−207.

(2) Washburn, M. P.; Wolters, D.; Yates, J. R. *Nat. Biotechnol.* **2001**, *19*, 242−247.

(3) Shen, Y. F.; Kim, J.; Strittmatter, E. F.; Jacobs, J. M.; Camp, D. G.; Fang, R. H.; Tolie, N.; Moore, R. J.; Smith, R. D. *Proteomics* **2005**, *5*, 4034−4045.

(4) Pappin, D. J. C.; Hojrup, P.; Bleasby, A. J. *Curr. Biol.* **1993**, *3*, 327−332.

(5) Henzel, W. J.; Billeci, T. M.; Stults, J. T.; Wong, S. C.; Grimley, C.; Watanabe, C. *Proc. Natl. Acad. Sci. U.S.A.*. **1993**, *90*, 5011−5015.

(6) Mann, M.; Hojrup, P.; Roepstorff, P. *Biol. Mass Spectrom.* **1993**, *22*, 338−345.

(7) Wilkins, M. R.; Lindskog, I.; Gasteiger, E.; Bairoch, A.; Sanchez, J. C.; Hochstrasser, D. F.; Appel, R. D. *Electrophoresis* **1997**, *18*, 403−408.

(8) Papayannopoulos, I. A. *Mass Spectrom. Rev.* **1995**, *14*, 49−73.

(9) Dongre, A. R.; Jones, J. L.; Somogyi, A.; Wysocki, V. H. *J. Am. Chem. Soc.* **1996**, *118*, 8365−8374.

(10) Huang, Y. Y.; Triscari, J. M.; Tseng, G. C.; Pasa-Tolic, L.; Lipton, M. S.; Smith, R. D.; Wysocki, V. H. *Anal. Chem.* **2005**, *77*, 5800−5813.

(11) Koeniger, S. L.; Merenbloom, S. I.; Valentine, S. J.; Jarrold, M. F.; Udseth, H.; Smith, R.; Clemmer, D. E. Submitted to *Anal. Chem*.

(12) Badman, E. R.; Myung S.; Clemmer, D. E. *Anal. Chem.* **2002**, *74*, 4889−4894.

(13) Kelleher, N. L.; Lin, H. Y.; Valaskovic, G. A.; Aaserud, D. J.; Fridriksson, E. K.; McLafferty, F. W. *J. Am. Chem. Soc.* **1999**, *121*, 806−812.

(14) Zubarev, R. A.; Horn, D. M.; Fridriksson, E. K.; Kelleher, N. L.; Kruger, N. A.; Lewis, M. A.; Carpenter, B. K.; McLafferty, F. W. *Anal. Chem.* **2000**, *72*, 563−573.

(15) Stephenson, J. L.; McLuckey, S. A. *Anal. Chem.* **1998**, *70*, 3533−3544. Pitteri, S. J.; McLuckey, S. A. *Mass Spectrom. Rev.* **2005**, *24*, 931−958.

10.1021/ac052208e CCC: $33.50
Published on Web 03/08/2006

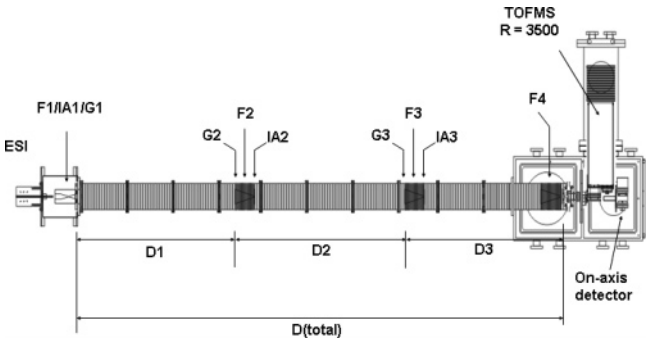

Figure 1. Schematic of the IMS−IMS−IMS-TOF instrument. Ions can be gated (G1−G3) and activated (IA1−IA3) in three regions of the instrument. See text for details.

shift high-charge-state ions to higher m/z regions of the spectra by reducing the charge.

EXPERIMENTAL SECTION

General Procedures. Figure 1 shows a schematic diagram of the IMS instrument used for these studies. Details of IMS theory and instrumentation (including the IMS−IMS−IMS−MS instrument used here) are described elsewhere;[11,16−21] only a short description of the instrumentation utilized for these studies is outlined here. Briefly, a continuous beam of electrosprayed ions is introduced directly into an ion funnel region (F1) and accumulated. Periodically the concentrated ion packet is gated into the first drift tube (D1). The drift tube contains ~3 Torr He buffer gas; ions migrate across the tube under the influence of a weak electric field, and different species separate due to differences in their mobilities through the gas. As ions exit the first drift region, they enter another ion funnel that is used to radially focus the diffuse ion clouds and transmit species into the front of a second drift region (D2). The entrance of D2 contains an ion gate and ion activation region such that it is possible to select and energize specific components of the ion mixture. There is a third drift region (D3) that operates in an analogous fashion. Ions exit the drift tube into a vacuum chamber and are focused into a time-of-flight mass spectrometer for m/z analysis.

The entire drift tube assembly is ~290 cm long; drift regions are operated at 9 V·cm^{-1}, the fields through the funnels are 11 V·cm^{-1}, and rf fields range from 70 to 100 V_{p-p} and 450 to 480 kHz. Ions are selectively gated by raising or lowering fields in the gate regions, as shown in Figure 1 at specific delay times that are controlled by a pulse delay generator (model DG535, Stanford Research Systems, Inc.). Collisional activation in any activation region (IA1, IA2, or IA3) is achieved by increasing the voltage between the last two lenses of each funnel.

Electrospray Source Conditions. Insulin chain B (Sigma, ≥80% purity) or ubiquitin (Sigma, 90% purity) was diluted to ~10^{-5} M in a 49:49:2 (% volume) solution of water/acetonitrile/acetic acid. Ions are emitted from a pulled capillary tip (75 μm i.d. × 360 μm o.d.), at a solution flow rate of 0.25 μL·min^{-1}, controlled by a syringe pump (KD Scientific, Holliston, MA). The pulled capillary was held at a dc bias 2 kV above the drift voltage. A PEEK microtee was used to couple the capillary tip, the syringe, and a platinum electrode.

RESULTS AND DISCUSSION

Analysis of a 30-Residue Peptide (ICB). Figure 2 (left) shows a typical nested IMS−MS [$t_D(m/z)$] distribution that is obtained when all regions of the drift tube are set to transmit all ions formed by electrospraying a solution of ICB. Although a number of features are observed, for the purposes of this paper, we limit our discussion to the two main charge states that are labeled: the broad distribution corresponding to the $[M + 4H]^{4+}$ ion at ~28 ms and two features at ~31 and 37 ms corresponding to different conformations of the $[M + 3H]^{3+}$ ion. By employing the delay generator and selection procedure (described above), it is possible to transmit a narrow region of ions having a specific mobility. Figure 2 (middle) illustrates this. Here, a narrow region of the broad peak associated with the $[M + 4H]^{4+}$of ICB (centered at 28.572 ms and $m/z = 874.42$) is transmitted into D2 and allowed to migrate through the rest of the instrument. This selection is carried out with no collisional activation, and thus, the spectrum is dominated by a sharp peak associated with the $[M + 4H]^{4+}$ ion.

Figure 2 (right) illustrates the ability to select and collisionally activate ions prior to further IMS separation. Here, the narrow $[M + 4H]^{4+}$ distribution is exposed to energizing conditions in IA2, and many different fragment ions are formed. A key aspect of the present work is that fragment ions separate in the D2 and D3 regions before exiting the drift tube for MS analysis. This is analogous in many ways to the IMS−MS analysis of ICB fragment ions that were formed by collisional activation in an ion trap that we presented previously; however, we note here that there is much greater ion signal, as well as higher mobility resolution such that many more features can be observed here (compared to the earlier report).[12]

The fragments that are observed in Figure 2 (right) appear to separate into families of ions that fall roughly along lines having similar m/z to t_D ratios. This is similar in many ways to observation of +1, +2, and higher charge-state families obtained upon analyzing protease digests.[22] In this case, as shown below, the patterns that are observed allow us to extract mass spectra associated with the +1 to +3 charge states, as well as some specific types of fragments (described in more detail below). Specific regions, highlighted by lines in Figure 2 (right), are examined in more detail.

The plots in Figure 3 make it possible to examine the patterns of peaks that are obtained upon mobility separation of the

(16) Revercomb, H. E.; Mason, E. A. *Anal. Chem.* **1975**, *47*, 970−983. Mason, E. A.; McDaniel, E. W. *Transport Properties of Ions in Gases*; Wiley: New York, 1988.
(17) St. Louis, R. H.; Hill, H. H. *Crit. Rev. Anal. Chem.* **1990**, *21*, 321−355.
(18) Mesleh, M. F.; Hunter, J. M.; Shvartsburg, A. A.; Schatz, G. C.; Jarrold, M. F. *J. Phys. Chem.* **1996**, *100*, 16082−16086. Shvartsburg, A. A.; Jarrold, M. F. *Chem. Phys. Lett.* **1996**, *261*, 86−91. Shvartsburg, A. A.; Hudgins, R. R.; Dugourd, P.; Jarrold, M. F. *Chem. Soc. Rev.* **2001**, *30*, 26−35.
(19) Wyttenbach, T.; von Helden, G.; Batka, J. J., Jr.; Carlat, D.; Bowers, M. T. *J. Am. Soc. Mass Spectrom.* **1996**, *8*, 275−282. Wyttenbach, T.; Bowers, M. T. *Mod. Mass Spectrom. Top. Curr. Chem.* **2003**, *225*, 207−232.
(20) Clemmer, D. E.; Jarrold, M. F. *J. Mass Spectrom.* **1997**, *32*, 577−592. Hoaglund Hyzer, C. S.; Counterman, A. E.; Clemmer, D. E. *Chem. Rev.* **1999**, *99*, 3037−3079.
(21) Collins, D. C.; Lee, M. L. *Anal. Bioanal. Chem.* **2002**, *372*, 66−73.
(22) Valentine, S. J.; Counterman, A. E.; Hoaglund, C. S.; Reilly, J. P.; Clemmer, D. E. *J. Am. Soc. Mass Spectrom.* **1998**, *9*, 1213−1216. Taraszka, J. A.; Counterman, A. E.; Clemmer, D. E. *Fresenius J. Anal. Chem.* **2001**, *369*, 234−245.

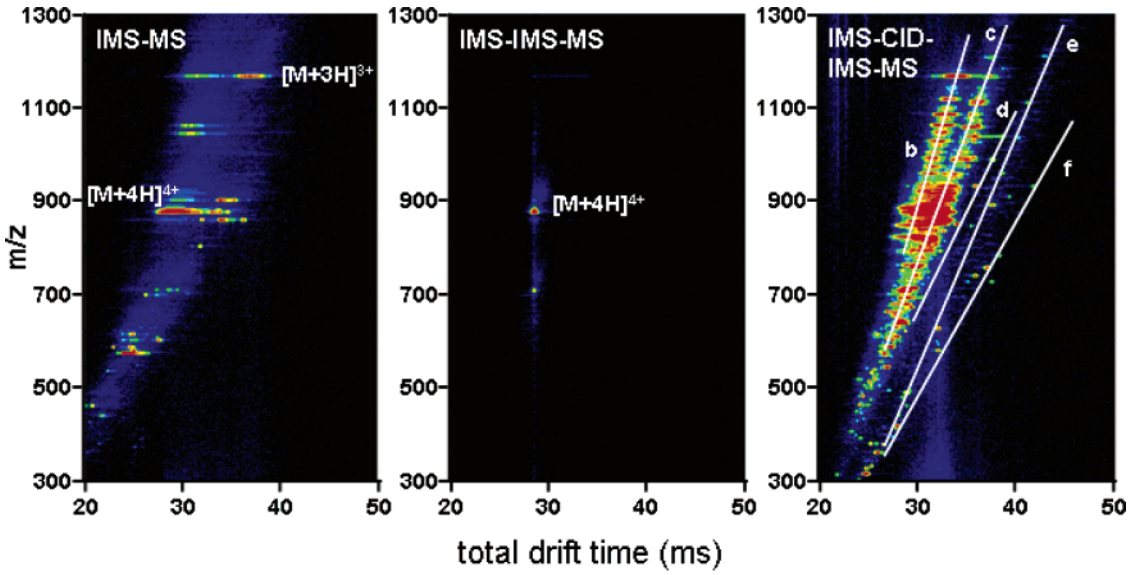

Figure 2. Two-dimensional $t_D(m/z)$ plot of electrosprayed insulin chain B precursor ions (left plot). The triply and quadruply charged ions are labeled. The middle plot shows the mobility-selected $[M + 4H]^{4+}$ ions obtained by gating a 50-μs-wide pulse of ions into the D2 region. The plot on the right shows the two-dimensional ion distribution obtained after collisionally activating the $[M + 4H]^{4+}$ ions in the second ion activation region (IA2). Diagonal lines correspond to mass spectra of fragment ion families shown in Figure 3.

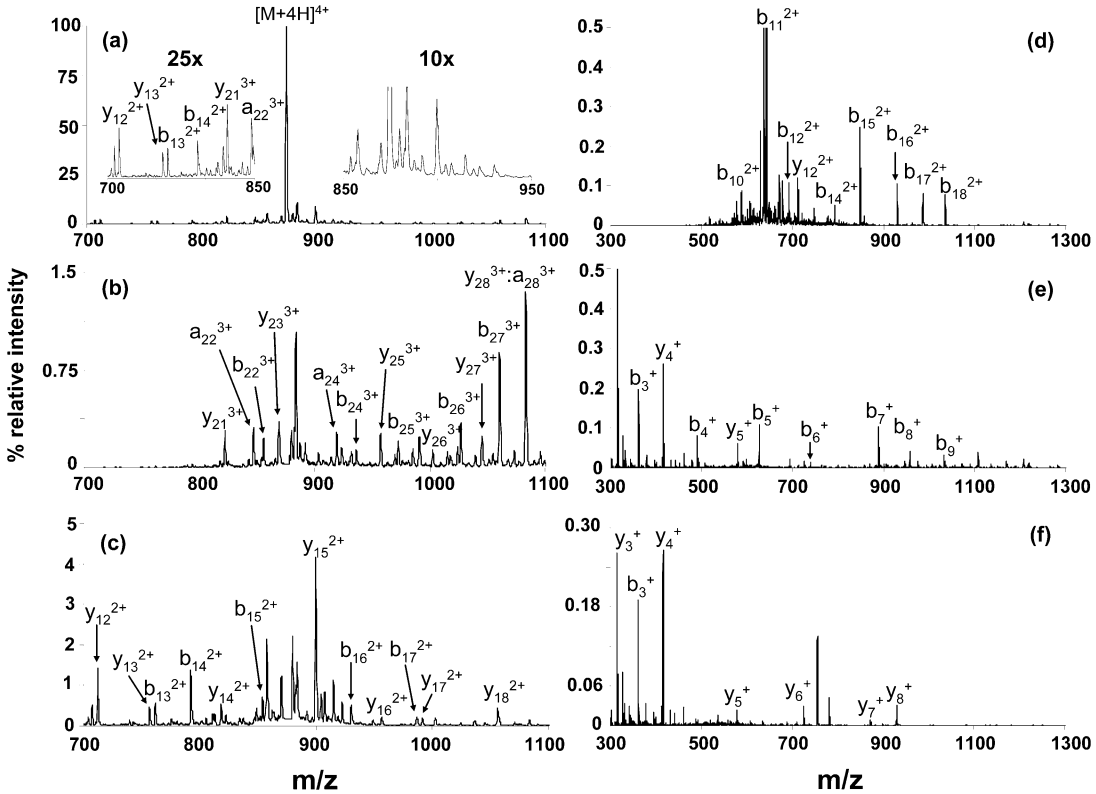

Figure 3. Mass spectra resulting from fragmentation of the $[M + 4H]^{4+}$ ion of insulin chain B. Plot a is the total ion mass spectrum obtained by integrating m/z values across the entire drift dimension. Plots b−f correspond to mass spectra extracted from the specific regions shown in Figure 2. These plots are obtained by integrating m/z values across narrow drift ranges centered about the diagonal lines. All mass spectra are normalized to the parent peak intensity. The fragments observed in all six mass spectra are summarized in Table 1.

fragments in more detail. There are several points that are noteworthy. From Figure 3a (which corresponds to the total integrated mass spectrum that would be obtained with no mobility separation), we notice that, under the conditions employed, fragmentation is a relatively inefficient process. The intensities of even the largest fragment peaks are still a factor of 20 times smaller than the precursor peak. There are two insets: one showing a blowup of the fragmentation region from 700 to 850, in which it is possible to identify several y- and b-ion fragments, and a second region from 850 to 950 that illustrates the overall level of the background signal. Near $m/z = 900$, the background signal level is relatively small (~2000 times less than the maximum of the precursor peak intensity), but still significant when compared to the low fragment peak intensities. From a careful

Table 1. Features Observed for Electrosprayed ICB Including Fragment Ion Assignments

m/z (unassigned features)[b]	fragment ion assignments [ion(*m/z* observed, *m/z* calculated)[a]]			
	a series	b series	y series	internal fragments[c]
300.35	a_4^+(461.11,461.25)	***b_3^+(361.22361.19)***	***y_3^+(315.37,315.20)***	F_{25}:P_{28}^+(510.01,509.59)
303.30	a_6^+(711.89,711.39)	b_4^+(489.98,489.25)	y_5^+(579.00,579.31)	Q_4:$C_7-NH_3^+$(513.00,513.55)
317.39	***a_7^+(862.42,862.39)***[d]	b_5^+(625.92,626.31)	***y_4^+(416.23,416.25)***	G_{20}:$F_{24}-28^+$(519.02,519.58)
327.34	a_9^{2+}(504.89,504.90)	b_6^+(738.91,739.39)	y_6^+(725.93,726.38)	C_{19}:$G_{23}-28^+$(523.77,523.55)
332.26	a_{10}^{2+}(571.89,572.25)	b_7^+(889.71,890.38)	y_7^+(873.02,873.45)	L_{11}:L_{15}^+(526.23,526.66)
342.21	***a_{11}^{2+}(628.93,628.80)***	b_9^+(1033.93,1034.40)	***y_8^+(930.27,930.47)***	G_{20}:$F_{24}-H_2O^+$(529.27,529.58)
378.18	***a_{12}^{2+}(678.44,678.33)***	***b_{10}^+(1170.78,1171.50)***	***y_9^{2+}(543.44,543.70)***	S_9:$E_{13}-H_2O^+$(548.01,548.62)
395.16	a_{18}^{3+}(681.57,682.02)	***b_{11}^+(1285.17,1284.58)***	***y_{10}^{2+}(608.52,608.31)***	L_{17}:E_{21}^+(550.23,550.61)
400.19	***a_{22}^{3+}(846.92,846.40)***	***b_{10}^{2+}(585.86,586.25)***	***y_{11}^{2+}(636.38,636.82)***	F_{24}:T_{27}^+(560.04,559.65)
413.15	***a_{24}^{3+}(914.74,914.43)***	***b_{11}^{2+}(642.44,642.79)***	***y_{12}^{2+}(711.89,712.32)***	Q_4:G_8^+(587.84,587.64)
431.15	***a_{26}^{3+}(1018.35,1017.81)***	***b_{12}^{2+}(691.82,692.33)***	y_{13}^{2+}(761.73,761.85)	G_8:$E_{13}-28^+$(595.82,595.68)
441.16	***a_{28}^{3+}(1083.44,1083.84)***	***b_{13}^{2+}(756.34,756.85)***	***y_{14}^{2+}(818.32,818.40)***	V_{18}:$G_{23}-28^+$(622.45,622.68)
494.04		***b_{14}^{2+}(791.81,792.37)***	***y_{15}^{2+}(899.71,899.93)***	***C_{19}:$F_{24}-28^+$(670.90,670.73)***
536.11		b_{15}^{2+}(848.76,848.91)	***y_{16}^{2+}(956.26,956.47)***	G_{20}:$F_{25}-NH_3^+$(677.95,677.74)
604.94		***b_{16}^{2+}(930.27,930.44)***	***y_{17}^{2+}(991.33,991.99)***	G_{23}:$P_{28}-28^+$(685.86,685.81)
629.40		***b_{17}^{2+}(986.76,986.98)***	***y_{18}^{2+}(1056.38,1056.51)***	L_{17}:$R_{22}-H_2O^+$(689.00,688.79)
647.41		***b_{18}^{2+}(1036.36,1036.52)***	***y_{19}^{2+}(1106.22,1106.14)***	L_{17}:R_{22}^+(707.18,706.80)
842.88		***b_{19}^{2+}(1112.31,1112.01)***	y_{20}^{2+}(1162.80,1162.59)	S_9:$L_{15}-H_2O^+$(732.41,732.86)
863.72		b_{20}^{2+}(1140.93,1140.53)	***y_{17}^{3+}(661.45,661.66)***	F_{24}:$K_{29}-28^+$(757.00,756.93)
879.75		b_{21}^{2+}(1205.39,1205.05)	***y_{18}^{3+}(704.16,704.68)***	H_5:$L_{11}-28^+$(768.72,768.88)
919.14		b_{17}^{3+}(658.21,658.32)	y_{20}^{3+}(775.21,775.39)	E_{21}:$Y_{26}-H_2O^+$(781.90,782.88)
949.24		b_{18}^{3+}(691.82,691.35)	***y_{21}^{3+}(822.30,821.08)***	***E_{21}:Y_{26}^+(800.90,800.90)***
963.30		b_{20}^{3+}(761.39,761.85)	y_{23}^{3+}(869.11,869.10)	G_8:L_{15}^+(808.00,807.93)
985.37		b_{22}^{3+}(855.76,855.73)	***y_{25}^{3+}(957.23,957.12)***	Q_4:H_{10}^+(811.30,811.86)
1015.33		b_{24}^{3+}(923.93,923.76)	***y_{26}^{3+}(1002.69,1002.81)***	***E_{13}:$C_{19}-28^+$(812.73,812.97)***
1073.49		***b_{25}^{3+}(972.73,972.79)***	***y_{27}^{3+}(1045.33,1045.50)***	G_{23}:$K_{29}-NH_3^+$(825.00,824.96)
1164.30		***b_{26}^{3+}(1027.03,1027.14)***	***y_{28}^{3+}(1083.44,1083.51)***	C_7:A_{14}^+(845.40,845.91)
		b_{27}^{3+}(1060.7,1060.82)	***y_{29}^{3+}(1116.32,1116.53)***	***G_{20}:Y_{26}^+(857.80,857.95)***
				L_{11}:$V_{18}-28^+$(874.33,874.12)
				E_{21}:$T_{27}-H_2O^+$(883.69,883.99)
				N_3:$H_{10}-H_2O^+$(907.31,907.00)
				H_{10}:$L_{18}-H_2O^+$(922.39,922.12)
				E_{21}:$P_{28}-NH_3^+$(981.81,982.09)
				C_{19}:$Y_{26}-H_2O^+$(990.93,991.08)
				S_9:$L_{17}-H_2O^+$(1009.70,1009.20)
				H_{10}:V_{18}^+(1039.41,1039.27)
				H_5:$A_{14}-28^+$(1067.91,1068.20)
				V_{18}:$Y_{26}-NH_3^+$(1090.94,1091.19)
				H_5:A_{14}^+(1095.95,1096.21)
				L_6:$Y_{16}-28^+$(1207.80,1207.40)

[a] Calculated *m/z* values have been obtained (using monoisotopic masses) from the program ms-product at http://prospector.ucsf.edu/ucsfhtml4.0/msprod.htm. [b] Mass-to-charge values have been obtained from the two-dimensional [$t_D(m/z)$] ICB data set. Only features with intensities higher than 3% of the base peak are listed here. In total, 52 features have not been assigned. [c] Internal fragment ions are listed as ***N-terminal residue:C-terminal residue***. [d] Features that can be identified from a single, total-ion mass spectrum are shown in italicized boldface type.

analysis of the total fragmentation mass spectrum, it is possible to discern 71 peaks, of which 50 can be assigned to fragments expected for the dissociation of ICB. A summary of the fragment ions observed is provided in Table 1.

As noted in previous reports, one of the advantages of mobility separations is the ability to observe many features that cannot be observed with MS alone.[22] Figure 3 shows mass spectra that are obtained by taking narrow slices along the lines indicated in Figure 2 (right). The data shown in Figure 3b and c correspond to narrow slices associated with the most intense fragments. Figure 3b (the highest mobility family) corresponds to a relatively intense series of +3 y- and b-ion fragments. Figure 3c corresponds to primarily +2 fragments of both y- and b-ion types. Many of the peaks that are observed from these slices (e.g., the $y_{21}^{3+}-y_{25}^{3+}$ and $y_{12}^{2+}-y_{17}^{2+}$ series, in Figures 3b and c, respectively) are also observed in the total mass spectrum (Figure 3a). Although not required for assignments, in these cases, the mobility separation aids the assignment by separating species according to the charge state (and reducing interference between these relatively large signals).

The mass spectra shown in Figure 3d–f illustrate how the mobility separation makes it possible to detect many peaks that are not detected by MS alone. The slice in Figure 3d picks up a series of small peaks with slightly longer drift times than the slice dominated by the +2 y-ion series in Figure 3c. An interesting aspect of this slice is that we assign the peaks primarily to a series of b ions ($b_{10}^{2+}-b_{18}^{2+}$). Only a single y ion (y_{12}^{2+}) is observed in this slice; however, this ion is actually centered in slice c (Figure 2) and is picked up in the slice d spectrum as the tail of the peak. Thus, in this spectrum, we observe a mobility family that is essentially exclusive to doubly charged b-type ions. The spectra shown in Figure 3e and f indicate that a similar behavior is observed in +1 fragments. In these spectra, there are regions above *m/z* values of ~600 that are associated with either +1 b-type or y-type ions. These data are the first to show clearly resolved regions for specific fragment types, a result that is intriguing in light of emerging de novo sequencing strategies.[23]

Although the representative slices through the IMS–MS data shown in Figure 3 are useful in illustrating the ability to see small

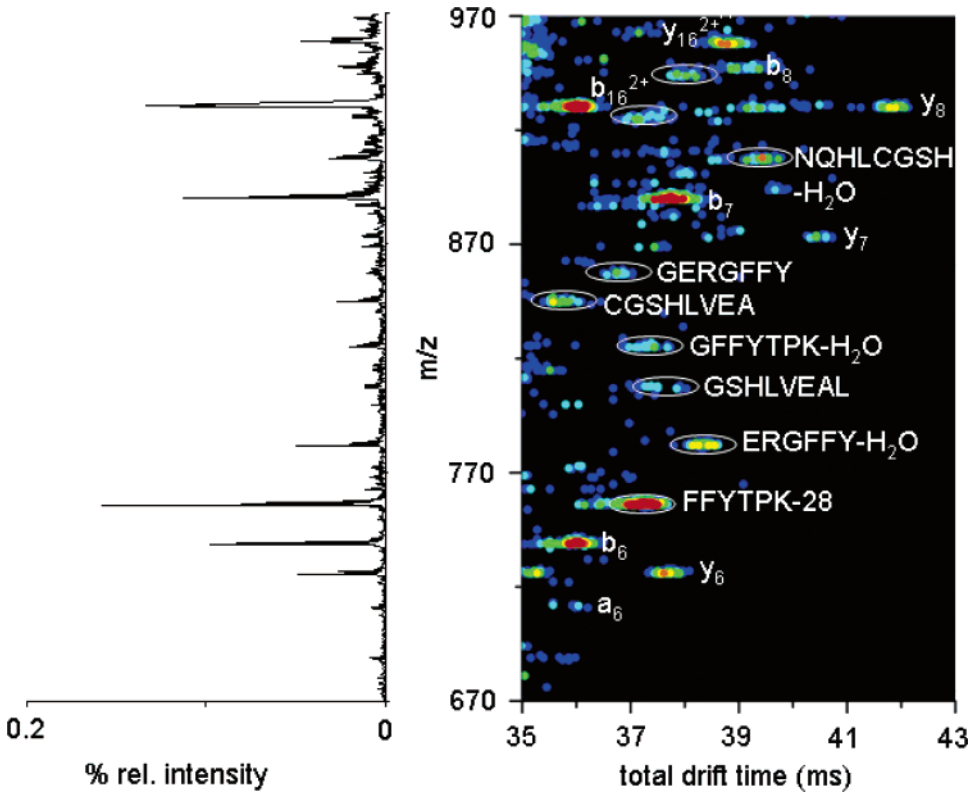

Figure 4. Narrow region of the nested $t_D(m/z)$ data set shown in Figure 2 (right). Mobility-separated fragment ions formed from $[M + 4H]^{4+}$ at IA2 are separated in drift space allowing identification of low-abundance ions. Several fragment ions are labeled, and internal fragment ions that were identified are circled. The integrated mass spectrum for the corresponding data is also shown normalized to the total integrated mass spectrum (Figure 3a).

features, it is also instructive to examine a low-intensity region directly. Figure 4 shows a narrow region of the spectrum (over a drift time range of 35−43 ms and $m/z = 670-970$). This region corresponds primarily to low-mobility +1 fragments (although the b_{16}^{2+} and y_{16}^{2+} fragments are also apparent). A careful analysis of these low-abundance features allows several additional peaks to be assigned. In particular, it appears that we have observed a number of very small features associated with internal fragments (as labeled). These features do not fall clearly into a family and thus are best represented in a two-dimensional plot. A complete analysis of the two-dimensional IMS−MS fragmentation spectrum in Figure 2 provides evidence for 170 peaks that have led to the 108 assignments that are given in Table 1. In this case, the mobility separation provides a 2-fold increase in the number of assigned peaks.

Analysis of a Larger System: Ubiquitin. Ubiquitin is a small, 76-amino acid protein that has been studied extensively.[14,23−27] Its size, combined with its being a well-characterized system, make ubiquitin a model protein to examine here. Figure 5 (left) shows an IMS−MS distribution of electrosprayed ubiquitin. This system exhibits a range of charge states ($[M + 6H]^{6+}$ to $[M + 13H]^{13+}$) and conformations (compact, partially folded, and elongated) as we have discussed previously.[24−26] Although we do not discuss it further here, it is straightforward to determine cross sections for distributions such as these and to select ions having specific mobilities. For convenience, at G2 we have selected a narrow window of ions having a total drift time of 33.86 ms. This selected distribution is shown in Figure 5 (right) and corresponds primarily to a broadly defined elongated conformation type of $[M + 13H]^{13+}$ ions (and a smaller population of the elongated $[M + 12H]^{12+}$ species).

Figure 6 shows the distribution of fragments that is obtained upon activation (at IA2) of the elongated $[M + 13H]^{13+}$ and $[M + 12H]^{12+}$ selected ions. In this case, a narrow range of mobility-selected species is collisionally activated at IA2 and the distribution of new ions that is formed is separated in the remaining portion of the instrument. This activation generates a range of new species, including a distribution of lower charge states that are formed by proton transfer (the $[M + 12H]^{12+}-[M + 6H]^{6+}$ ions that are shown) as well as a series of fragment ions. Using previous assignments,[14,27] we can readily identify two fragment series: the $b_{14}^{3+}-b_{18}^{3+}$ ions and a series of $y_{55}^{9+}-y_{59}^{9+}$ ions. It is possible to select any number of these fragments at G3 for further study. As an example, we have selected the y_{58}^{9+} ion (Figure 6, center). It is worth noting that the IMS−MS spectrum displayed corresponds to all ions; thus, the two selections result in a remarkably unique selection of the y_{58}^{9+} species. Figure 6 (right)

(23) Shevchenko, A.; Chernushevich, I.; Ens, W.; Standing, K. G.; Thomson, B.; Wilm, M., Mann, M. *Rapid Commun. Mass Spectrom.* **1997**, *11*, 1015−1024.
(24) Valentine, S. J.; Counterman, A. E.; Clemmer, D. E. *J. Am. Soc. Mass Spectrom.* **1997**, *8*, 954−961.
(25) Li, J.; Taraszka, J. A.; Counterman, A. E.; Clemmer, D. E. *Int. J. Mass Spectrom.* **1999**, *185/186/187*, 37−47.
(26) Myung, S.; Badman, E.; Lee, Y. J.; Clemmer, D. E. *J. Phys. Chem. A* **2002**, *106*, 9976−9982.
(27) Reid G. E.; Wu, J.; Chrisman, P. A.; Wells, J. M.; McLuckey, S. A. *Anal. Chem.* **2001**, *73*, 3274−3281.

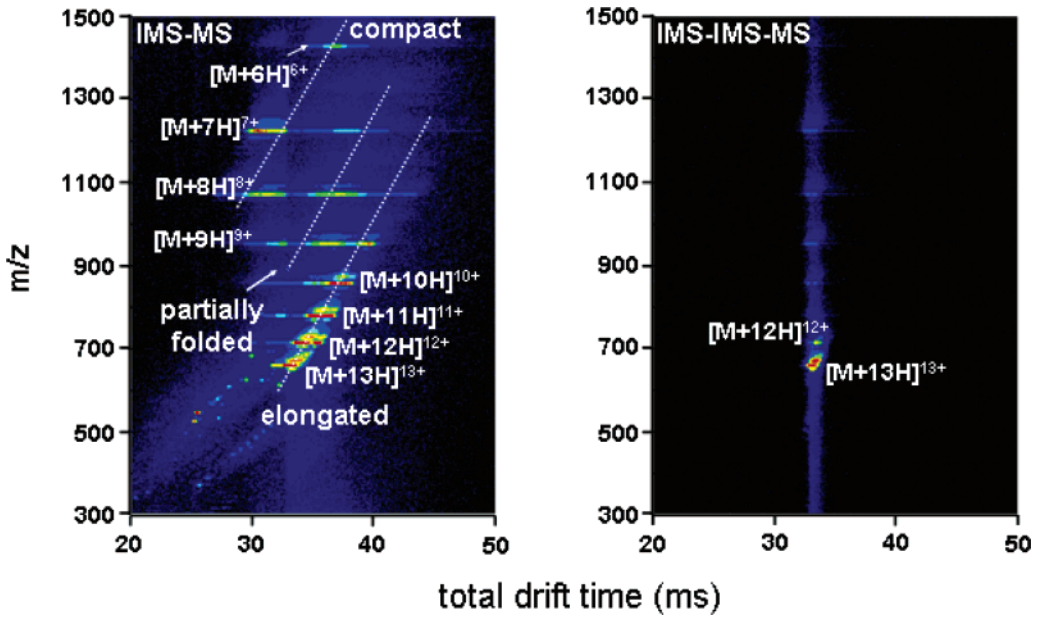

Figure 5. Two-dimensional $t_D(m/z)$ plot of electrosprayed ubiquitin ions obtained by allowing the entire distribution of ions to traverse D(total) (left). The $[M + 6H]^{6+}$–$[M + 13H]^{13+}$ charge states are observed, with conformations (compact, partially folded, and elongated, as defined previously) shown by lines. The $[M + 13H]^{13+}$ ion is isolated in the two-dimensional separation by mobility selection of ions centered at ~33.86 ms with a 50-μs-wide pulse at G2 (right).

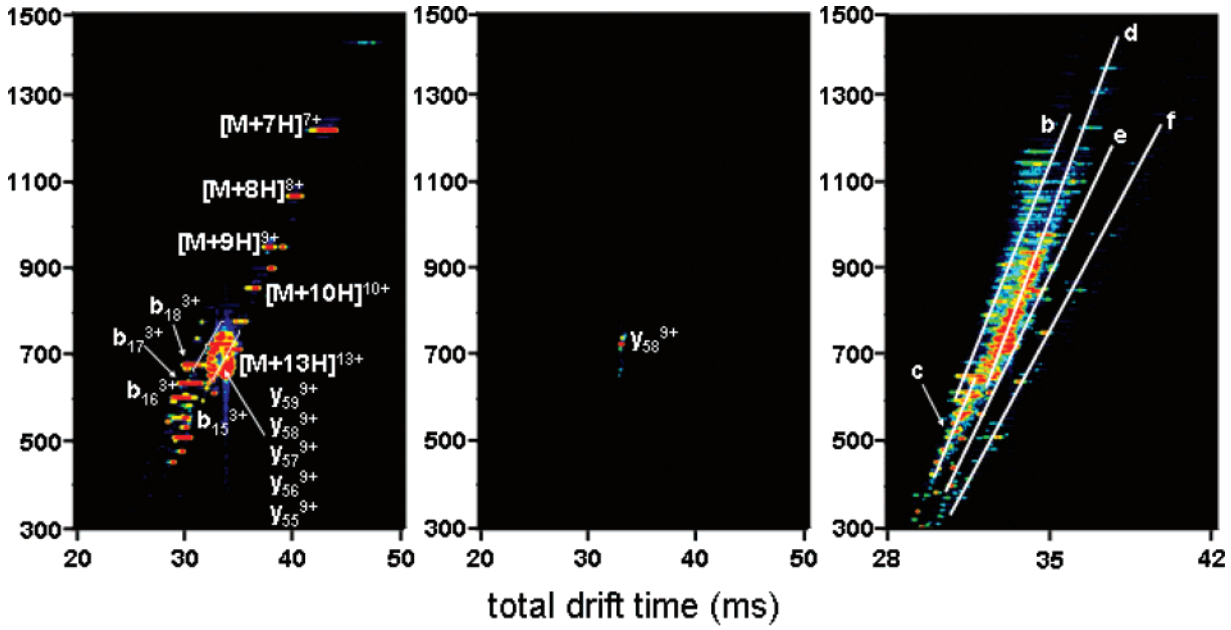

Figure 6. Two-dimensional $t_D(m/z)$ plot of mobility-dispersed fragment ions (left plot) obtained by selection of the $[M + 13H]^{13+}$ ion of electrosprayed ubiquitin at G2 and activation at IA2. Fragment ions formed upon activation of the $[M + 13H]^{13+}$ as well as charge states formed via charge transfer are shown. The y_{58}^{9+} fragment ion is mobility selected at G3 (middle plot). Fragment ions produced upon activation of the $(y_{58})^{9+}$ in IA3 are separated based on their mobilities through D3 (right plot). Diagonal lines correspond to mass spectra of fragment ion families shown.

shows a plot of IMS–MS data that is obtained when the selected y_{58}^{9+} ion is activated at IA3 and the fragments are separated again in D3. The result is a series of mobility-separated fragments.

As in the case of ICB (Figure 2), these ions fall into families according to similarities in m/z to t_D ratios. The lines that are shown in Figure 6 (right) illustrate five regions that we have shown as mass spectral slices in Figure 7. These data (Figure 7) illustrate a number of advantages that are similar to those described above for ICB. In this case, the y_{58}^{9+} precursor dominates the total integrated mass spectrum. While it is possible to observe and assign several a, b, and y fragments in the total ion mass spectrum, many features become more apparent when the IMS dimension is included. For example, Figure 7b shows a relatively low-intensity series of high-mobility fragments that includes a set of peaks that can be assigned to most of the b_{16}^{3+}–b_{29}^{3+} series. The mass spectra corresponding to the most intense fragments are shown as Figure 7c and d. Both of these slices contain a series of y^{3+} ions as well as some species that are attributed to higher charge states (that are expected to be observed as relatively high-mobility ions). The distributions shown in Figure 7e and f correspond to low-intensity features that are observed at lower m/z to t_D ratios. Figure 7e illustrates a region

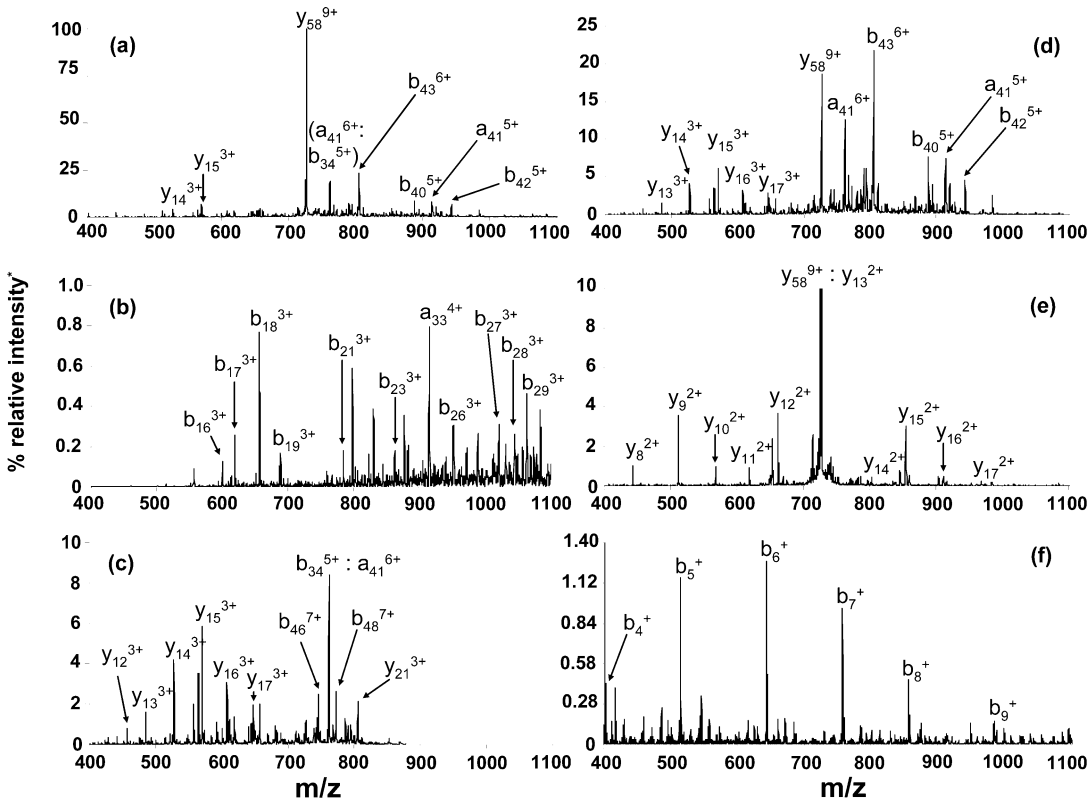

Figure 7. Mass spectra resulting from fragmentation of the y_{58}^{9+} fragment ion produced from the $[M + 13H]^{13+}$ of electrosprayed ubiquitin. Plot a is the total ion mass spectrum obtained by integrating *m*/*z* values across the entire drift dimension. Plots b−f correspond to mass spectra extracted from the specific regions shown in Figure 6. These plots are obtained by integrating *m*/*z* values across narrow drift ranges centered about the diagonal lines. All mass spectra are normalized to the parent peak intensity.

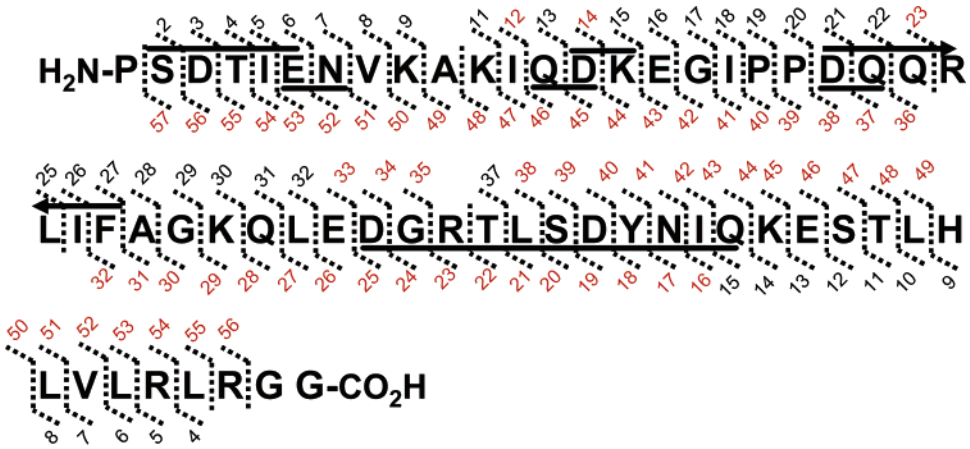

Figure 8. Amino acid sequence for the y_{58}^{9+} of ubiquitin, with bond cleavages of a- or b-and y-type ions shown as dotted lines. Fragments found in both the total ion mass spectrum (Figure 6a) and the diagonal slices (Figure 6b−f) are shown in black, while fragments observed in only the diagonal slices are shown in red. Internal fragments are underlined. In all, 64 additional unique ions are observed via examination of the mobility-dispersed fragments.

of the spectrum that is associated with primarily 2+ y ions, and we assign the y_8^{2+}−y_{17}^{2+} series. Similarly, a very low intensity series of singly charged, b-type ions (the b_4^+−b_9^+ series) are shown in Figure 7f. We note that b_2^+ and b_3^+ are also observed in this slice but are outside of the range that is shown.

The number of fragments and assignments that are made for the y_{58}^{9+} ion of ubiquitin is substantially larger than the number reported for ICB (summarized in Table 1). Due to size, we felt it unnecessary to present the complete analysis of ubiquitin as a table. Instead, we illustrate the sequence coverage obtained in these studies in Figure 8. Briefly, we assigned a total of 235 expected fragment ions upon examining the mobility-dispersed, charge-state- and fragment-specific families from fragmentation of the y_{58}^{9+} precursor. Many of these assignments correspond to relatively large fragments that are observed in several different charge states; for example, the y_{53} fragment has been observed with +7, +8, and +9 charges. In such cases, the mobility resolution aids in delineating components.

In total, Figure 8 shows that when coverage from all types of ions is considered, we find direct evidence for cleavage for nearly all residues in the y_{58}^{9+} sequence (either as b-, y-, or a-type ion, or an internal fragment). This includes a very complete series of

b- and y-type ions. Across all charge states, five b-type fragments are not observed: b_1, b_{10}, b_{24}, b_{36}, and b_{57}. Of the y-type ions, Figure 8 shows that only the $y_{33}-y_{35}$ ions are missing. This coverage takes advantage of many very small features that are apparent only in the IMS−MS distributions. For example, the same analysis for the fragments that are observed from the integrated mass spectra shows that, of the 114 possible b- and y-type ions (57 b-type and 57 y-type, respectively), 20 b-type and 39 y-type ions are not observed.

SUMMARY AND CONCLUSIONS

We have shown that IMS−MS analysis of fragment ions produced by collision-induced dissociation allows many peaks that would not be resolved by MS alone to be identified. The approach is effective because isobaric ions can often be separated based on differences in mobilities, allowing low-intensity features to be extracted from the data. The approach should be an effective tool for enhancing the ability to use fragmentation information to identify peptides and proteins in database searching methods.

An interesting finding is that some ion types (e.g., b and y ions) appear to fall into families. This suggests that these ions may form different types of structures, such as the helical and globular motifs that have been studied extensively as model systems.[20,28] At this point, we do not know how general this type of phenomenon may be. Work that is aimed at understanding the patterns of fragment ions (for specific fragment types and charge states) is ongoing.

(28) For example, see: Henderson, S. C.; Li, J.; Counterman, A. E.; Clemmer, D. E. *J. Phys. Chem. B* **1999**, *103*, 8780−8785. Counterman, A. E.; Clemmer, D. E. *J. Am. Chem. Soc.* **1999**, *121*, 4031−4039. Hudgins, R. R.; Jarrold, M. F. *J Am. Chem. Soc.* **1999**, *121*, 3494−3501. Kinnear, B. S.; Kaleta, D. T.; Kohtani, M.; Hudgins, R. R.; Jarrold, M. F. *J. Am. Chem. Soc.* **2000**, *122*, 9243−9256. Counterman, A. E.; Clemmer, D. E. *J. Am. Chem. Soc.* **2001**, *123*, 1490−1498. Taraszka, J. A.; Counterman, A. E.; Clemmer, D. E. *Int. J. Mass. Spectrom.* **2001**, *204*, 87−100. Counterman, A. E.; Clemmer, D. E. *J. Phys. Chem. B* **2002**, *106*, 12045−12051. Srebalus Barnes, C. A.; Clemmer, D. E. *J. Phys. Chem. A* **2003**, *107*, 10566−10579. Counterman, A. E.; Clemmer, D. E. *J. Phys. Chem. B* **2004**, *108*, 4885−4898.

ACKNOWLEDGMENT

This work is supported by grants from National Institutes of Health (AG-024527-01) and (P41. RR018942). We also acknowledge partial funding of this work from grants from the Analytical Node of the Indiana University MetaCyt initiative funded by the Lilly Endowment and the Indiana 21st Century Fund.

Received for review December 14, 2005. Accepted February 10, 2006.

AC052208E